Kinetic parameters for the reaction of OH radical initiated atmospheric oxidation of (E)-2-pentenal: *ab initio* and transition state theory calculations

B. Upendra, D. S. Lakshmi Prasanna and B. Rajakumar*

Department of Chemistry, Indian Institute of Technology Madras, Chennai 600 036, India

Kinetic parameters for the reaction of OH radical initiated atmospheric oxidation of (E)-2-pentenal were computed using *ab initio* methods, viz. G3MP2 coupled with conventional transition state theory with the Wigner tunnelling corrections in the temperature range 200–400 K. Every stationary point on the potential energy surface was obtained at MP2 (FULL)/6-31G* level of theory. Arrhenius rate expression for the title reaction with G3MP2 theory was computed to be $k = (2.57 \pm 0.33) \times 10^{-13} \exp[(1482 \pm 53)/T]$ cm^3 mol^{-1} s^{-1}. The OH-driven atmospheric lifetime of (E)-2-pentenal in the Earth's troposphere was calculated to be 5 h, with diurnally averaged concentration of OH radicals taken as 1.6×10^6 mol^{-1} cm^{-3}. The results obtained are in good agreement with the experimental results.

Keywords: *ab initio* methods, atmospheric oxidation, kinetic parameters, transition state theory.

Introduction

EMISSIONS of biogenic volatile organic compounds (BVOCs) into the Earth's atmosphere are larger than the anthropogenically emitted volatile organic compounds (VOCs). As BVOCs directly and indirectly take part in global warming and aerosol formation, they are detrimental to the ozone layer in the Earth's atmosphere[1–3]. BVOCs substantially contribute to the hydrocarbon load on atmosphere. Hence they were considered in the Kyoto Protocol policies regarding ecosystem, regional and countryside carbon dioxide budgets[4]. Major source of BVOCs is vegetation[5]. Emission of BVOCs occurs from the defence system of plants (wounded and cut plants) and plant–plant interactions[6]. Oxygenated VOCs are ubiquitous chemical constituents in the atmosphere[7]. These compounds can be biosynthesized from linoleic and α-linoleic acids[6] and exhibit antibacterial properties[8]. Clover and grass emits VOC rich in light oxygenates, like methanol, ethanol, acetaldehyde and butanone. Higher aldehydes have been observed in ambient air and various plant emissions. The atmospheric degradation of these compounds could influence in the tropospheric ozone production, secondary organic aerosol formation and air quality over all parts of the globe[9]. The atmospheric oxidation of these (carbonyl) compounds is mainly initiated by their reaction with OH radicals during daytime, and to a lesser extent, with the NO_3 radical during night-time[10]. Several studies on the reactions of OH radicals with molecules such as saturated and unsaturated aldehydes[11,12] and isoprene[13] have been reported earlier. The test molecule (E)-2-pentenal is one among many BVOCs emitted into the Earth's atmosphere. Reactions with OH radicals are major degradation processes of these BVOCs under atmospheric conditions. Thus, fundamental understanding of the chemical reactions between OH radicals and BVOCs is essential. Experimental studies for the reaction of (E)-2-pentenal with OH radical have been reported[14]. Davis *et al.*[10] and Albaladejo *et al.*[14] have measured the rate coefficient of the title reaction and reported the rate coefficient at 298 K to be $(2.48 \pm 0.24) \times 10^{-11}$ cm^3 mol^{-1} s^{-1}. Davis *et al.*[10] have measured the rate coefficients over the temperature range 244–374 K, and the reported rate expression is $k = (7.9 \pm 1.2) \times 10^{-12} \exp[(510 \pm 20)/T]$ and the coefficient is $(4.3 \pm 0.6) \times 10^{-11}$ cm^3 mol^{-1} s^{-1} at 297 K. To the best of our knowledge, the only one theoretical study by Grosjean and Williams[15] has been reported so far for the title reaction based on semi-empirical methods and rate coefficient at 298 K was found to be 2.9×10^{-11} cm^3 mol^{-1} s^{-1}.

In this study, we present the rate coefficients of the reaction of (E)-2-pentenal with OH radical in the temperature range 200–400 K using the conventional transition state theory (CTST) with Wigner tunnelling corrections coupled with the G3MP2 theory. All the possible channels for the reaction are given below.

$$CH_3CH_2CH{=}CHCHO + OH \rightarrow CH_3CH_2CH{=}CHCO + H_2O, \quad (C1)$$

$$CH_3CH_2CH{=}CHCHO + OH \rightarrow CH_3CH_2CH{=}CCHO + H_2O, \quad (C2)$$

*For correspondence. (e-mail: rajakumar@iitm.ac.in)

$$CH_3CH_2CH{=}CHCHO + OH \rightarrow CH_3CH_2C{=}CHCHO + H_2O, \quad (C3)$$

$$CH_3CH_2CH{=}CHCHO + OH \rightarrow CH_3CHCH{=}CHCHO + H_2O, \quad (C4)$$

$$CH_3CH_2CH{=}CHCHO + OH \rightarrow CH_2CH_2CH{=}CHCHO + H_2O. \quad (C5)$$

We report the structural and energetic parameters of all the reactants, transition states and the products in addition to the thermodynamic parameters of the title reaction. We present the vibrational frequencies of each stationary point, i.e. reactants, transition states and products. We also report the contribution of all the transition states to the global rate coefficient for the title reaction. The plausible degradation mechanism for the test molecule is discussed. Finally, the hydroxyl radical (OH)-driven atmospheric lifetime of the test molecule is reported.

Computational methods

All calculations were carried out by using GAUSSIAN-03 program suite[16]. Structures of reactants, transition states and products were optimized at Møller–Plesset[17] (MP2 (FULL)) level of theory with Pople 6-31G* basis set, by using internally available Gaussian package. The potential energy surface (PES) was scanned at the reported theory and two rotamers were found for the test molecule, designated as R1 and R2. Each rotomer was identified with eight different transition states and designated as R1-TS1, R1-TS2, R1-TS3, R1-TS4, R1-TS5, R1-TS6, R1-TS7, R1-TS8 and R2-TS1, R2-TS2, R2-TS3, R2-TS4, R2-TS5, R2-TS6, R2-TS7, R2-TS8. Here TS1 corresponds to the abstraction of hydrogen from the aldehyde group; TS2 corresponds to the abstraction of hydrogen from the methyne (=CH–) group; TS3 corresponds to the abstraction of hydrogen from the methyne (=CH–) group next to the $–CH_2–$ group; TS4 and TS5 correspond to abstraction of hydrogen from the methylene ($–CH_2–$) group and TS6–TS8 correspond to abstraction of hydrogen from the methyl ($–CH_3$) group. The prefixes R1 and R2 correspond to the rotamer '1' and '2' respectively. Frequency calculations were carried out for all reactants, transition states and products at the same level of theory and basis set. All the reactants and products were observed with the positive frequencies. All the transition states were identified with one imaginary frequency corresponding to the appropriate reaction coordinate, i.e. the processes of abstraction of hydrogen from the test molecule. The structures and normal modes were viewed in Gauss View[18] and the normal mode corresponding to the reaction coordinate was observed to be consistent with the reaction of interest. Structural parameters obtained from MP2 (FULL)/6-31G* level of theory were used in Gaussian-3 method[19], namely G3MP2 in order to get the energies of all the reactants, transition states and products, and these energies and geometries were used in the TST calculations.

Rate coefficients

Rate coefficients for hydrogen abstraction from (E)-2-pentenal by OH radical were calculated using CTST[20,21] at every 25 K within the complete temperature range, 200 and 400 K, with the reported theory.

$$k(T) = l\frac{k_B T}{h}\left(\frac{Q_{\ddagger}}{Q_R}\right)\exp\left(-\frac{\Delta E_0}{RT}\right),$$

where l is the statistical factor (reaction path degeneracy), k_B the Boltzmann constant, T the temperature and h is the Planck's constant. The symbol (‡) represents the transition state and R is the universal gas constant. ΔE_0 is the activation barrier and was calculated from the difference in energy between the transition state and the reactants. $Q_{\ddagger}$ and Q_R are the total partition functions of the transition state and reactants respectively. The total partition function is given by the product of translational, vibrational, rotational, electronic and internal–rotational (for lower normal mode frequencies) partition functions. Rotational constants and vibrational frequencies obtained at MP2 (FULL)/6-31G* level of theory were used to calculate the rotational and vibrational partition functions. The electronic partition function of the OH radical was evaluated by taking the splitting of 139.7 cm^{-1} in the $^2\Pi$ ground state into account[22].

$$Q^E(\mathrm{OH}) = 2 + 2\exp[-140\,(\mathrm{cm}^{-1})hc_0/k_B T],$$

where c_0 is the velocity of light in vacuum. Quantum mechanical tunnelling effect along the reaction coordinate was calculated by temperature dependent transmission coefficient $\Gamma(T)$. The values of $\Gamma(T)$ were calculated using Wigner empirical method[23] (see Table SIII in the Supporting Information). In this method, the transmission coefficient for tunnelling was calculated using the expression,

$$\Gamma(T) = 1 + \frac{1}{24}\left(\frac{h\nu^*}{k_B T}\right)^2, \quad (1)$$

where ν^* is the imaginary frequency of the transition state. The final rate coefficient was given by

$$k^{\Gamma}(T) = \Gamma(T)k(T). \quad (2)$$

Results and discussion

Electronic structure

The PES scan was carried out at MP2 (FULL)/6-31G* level of theory and two rotamers were found for the test

molecule ((E)-2-pentenal), designated as R1 and R2. The PES scan plotted between energy (Hartree) and angle (degree) is given in Figure 1. All the structures of reactant molecules, transition states and products optimized at MP2 (FULL)/6-31G* level of theory are shown in Figure 2. All the optimized structural parameters of reactants, transition states and the products are given in Table SI of the Supporting Information. Vibrational analyses were carried out and the vibrational frequencies obtained with the reported theory are given in Table SII of the Supporting Information. Imaginary frequencies in the transition states correspond to the abstraction of H by OH radical. In the transition state, the important structural parameters to be observed are, one of the C–H bonds of the leaving hydrogen and the newly formed bond between the H and O atoms. In Table 1, the differences in bond length of the C–H and O–H bonds between the transition state and the reactant are expressed as percentage relative to the reactant. The leaving C–H bond length seems to have varied from 7.5% to a maximum of 23.3% in case of all the transition states with the MP2(FULL)/6-31G* level of theory. However, in case of the newly formed bond, i.e. H–O bond, the bond length seems to have varied between 19.6% and 59.2%.

Energetics

The energies (in Hartree) of the reactant molecules, transition states and products computed with the reported theory are given in the Table SIII of the Supporting Information. The entropy of activation ($\Delta S^{\ddagger}$) and the classical barrier heights (ΔE_0) for the reaction are given in Table 2. The classical barrier heights were calculated from the energy (including ZPVE) difference between the transition state and reactant ($CH_3CH_2CH{=}CHCHO$ and OH) molecules. Energy-level diagrams for rotamers R1 and R2 are given in Figures 3 and 4 respectively. With the G3MP2 theory, all transition states are observed with positive barriers, except in the case of R1-TS1 and R2-TS1 (Table 2). The negative barrier height for R1-TS1 and R2-TS1 is attributed to one of the reaction pathways in which hydrogen attached to the aldehydic group, is abstracted. It is clear from Table 2 that ΔE_0 is negative for only the aldehydic hydrogen channel (–2.08 k cal mol^{-1}

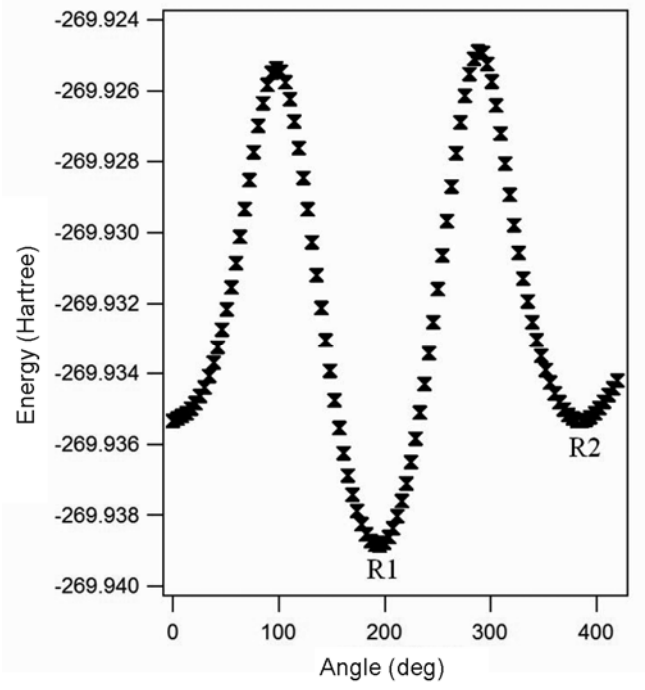

Figure 1. Potential energy diagram of $CH_3CH_2CH{=}CHCHO$ at MP2(FULL)/6-311++G** level of theory.

Table 1. Summary of C–H and O–H bond distances (Å) and % changes calculated for all the transition states for H abstraction from $CH_3CH_2CHCHCHO$ by OH radical

Transition state	Bond	Rotamer-1 MP2 (FULL)/ 6-31G*	Rotamer-2 MP2 (FULL)/ 6-31G*
TS1	C–H (RT)[a]	1.111	1.107
	O–H (RT)[b]	0.978	0.978
	C–H (TS)	1.195 (7.5%)	1.193 (+7.7%)
	O–H (TS)	1.419 (45%)	1.398 (42.8%)
TS2	C–H (RT)[a]	1.087	1.088
	O–H (RT)[b]	0.978	0.978
	C–H (TS)	1.286 (+18%)	1.255 (15.3%)
	O–H (TS)	1.171 (+19.6%)	1.207 (23.3%)
TS3	C–H (RT)[a]	1.092	1.090
	O–H (RT)[b]	0.978	0.978
	C–H (TS)	1.248 (+14.2%)	1.274 (+16.8%)
	O–H (TS)	1.233 (+26%)	1.182 (+20.1%)
TS4	C–H (RT)[a]	1.095	1.095
	O–H (RT)[b]	0.978	0.978
	C–H (TS)	1.206 (+10.2%)	1.202 (+9.7%)
	O–H (TS)	1.314 (+34%)	1.324 (+35.3%)
TS5	C–H (RT)[a]	1.097	1.097
	O–H (RT)[b]	0.978	0.978
	C–H (TS)	1.207 (+10%)	1.215 (+10.8%)
	O–H (TS)	1.302 (+33%)	1.284 (+31.2%)
TS6	C–H (RT)[a]	1.093	1.095
	O–H (RT)[b]	0.978	0.982
	C–H (TS)	1.219 (+11.6%)	1.239 (+13%)
	O–H (TS)	1.282 (+30.9%)	1.289 (+31.2%)
TS7	C–H (RT)[a]	1.093	1.095
	O–H (RT)[b]	0.978	0.982
	C–H (TS)	1.211 (+10.8%)	1.247 (+13.9%)
	O–H (TS)	1.303 (+33%)	1.284 (+30.6%)
TS8	C–H (RT)[a]	1.092	1.095
	O–H (RT)[b]	0.978	0.982
	C–H (TS)	1.213 (+11.1%)	1.250 (+14.6%)
	O–H (TS)	1.292 (+32%)	1.274 (+29.6%)

[a]C–H bond length (the leaving hydrogen) in the reactant.
[b]The actual O–H bond length in H_2O at the G3MP2 theory. Numbers given in parenthesis correspond to the % change in the bond length in the transition state compared to the same bond length in the reactant.

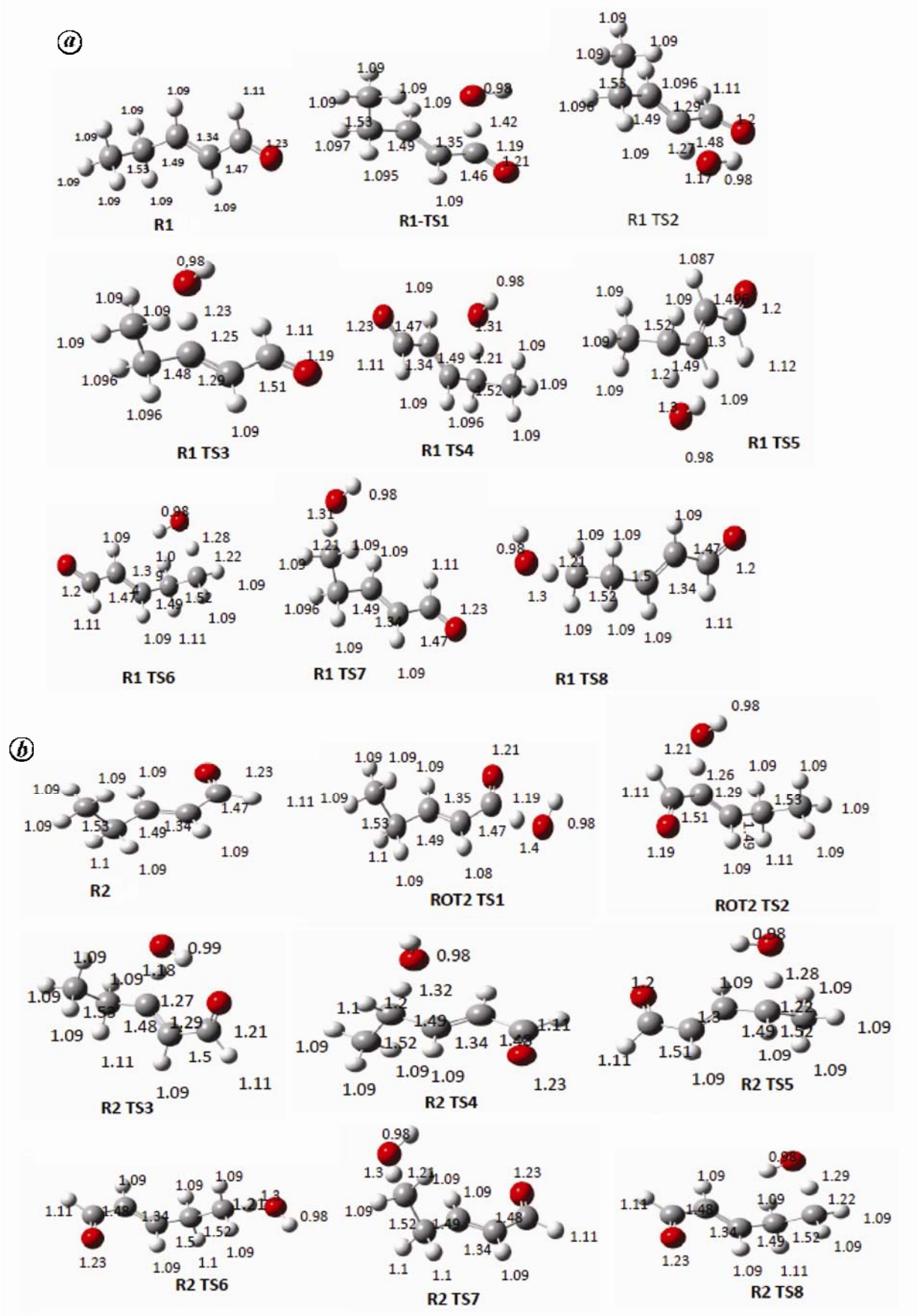
a
R1
R1-TS1
R1 TS2
R1 TS3
R1 TS4
R1 TS5
R1 TS6
R1 TS7
R1 TS8
b
R2
ROT2 TS1
ROT2 TS2
R2 TS3
R2 TS4
R2 TS5
R2 TS6
R2 TS7
R2 TS8

(*Contd*)

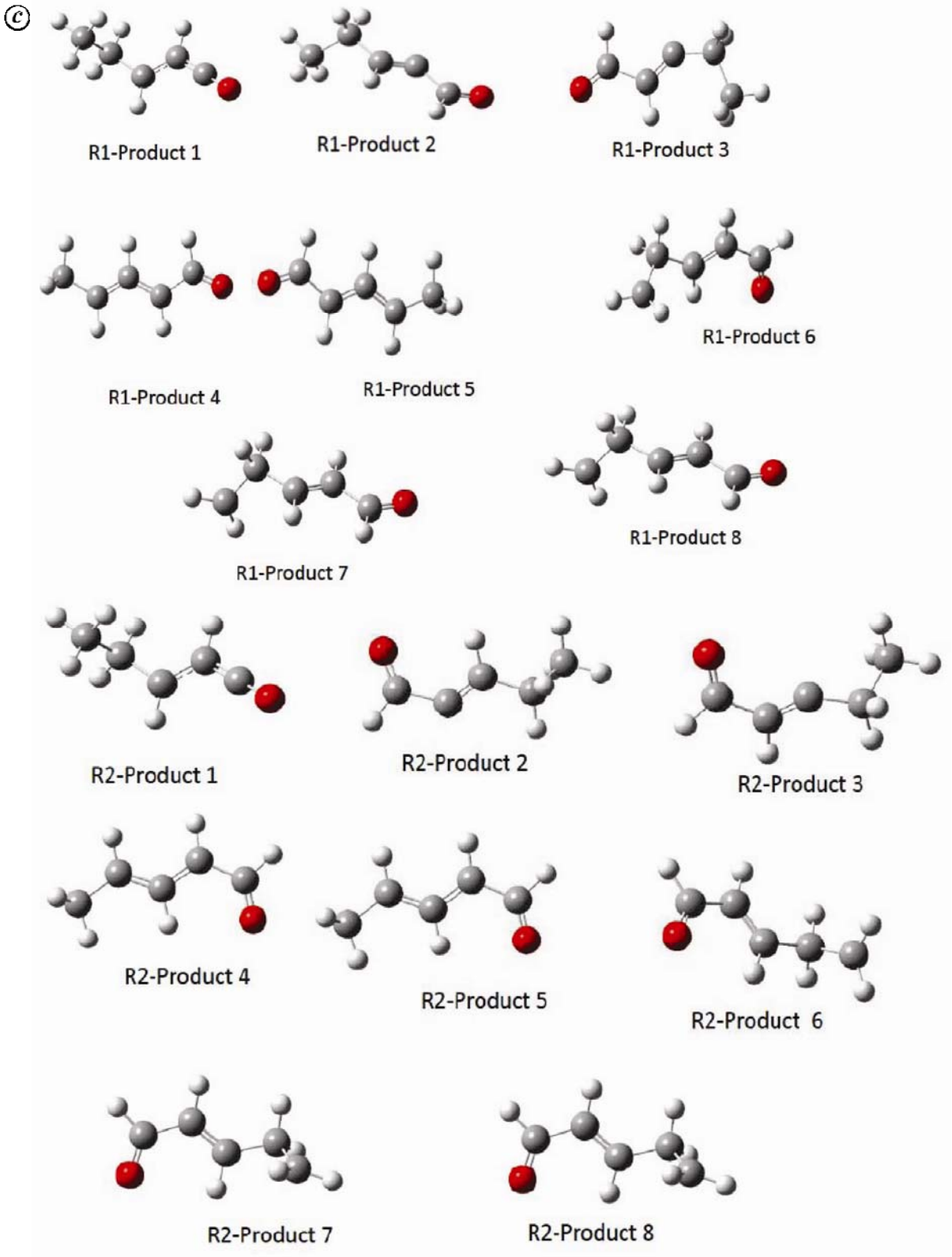

Figure 2. ***a***, Geometries of the reactant and transition states corresponding to rotamer-1 optimized at G3MP2 level of the theory. Grey represents carbon, white represents hydrogen and red represents oxygen atoms in the structures. The bond lengths (Å) given on the structures are obtained at G3MP2 theory. R1 denotes rotamer 1 and TS denotes transition state. ***b***, Geometries of the reactant and transition states corresponding to rotamer-2 optimized at G3MP2 level of the theory. Grey represents carbon, white represents hydrogen and red represents oxygen atoms in the structures. The bond lengths (Å) given on the structures are obtained at G3MP2 theory. R2 denotes rotamer 2. ***c***, Geometries of products optimized at G3MP2 level of the theory. Grey represents carbon, white represents hydrogen and red represents oxygen atoms in the structures. The bond lengths (Å) given on the structures.

in case of R1-TS1 and –1.56 k cal mol^{-1} in case of R1-TS2). Therefore it is obvious that the aldehydic hydrogen contributes maximum (discussed later in the article) towards the global rate coefficient. The lower barrier heights in case of R1-TS5 and R2-TS5 (Table 2) may be due to the abstraction of hydrogen from the methylene (–CH_2–) group which is relatively highly acidic in nature. The standard enthalpy change, standard free energy and standard entropy change obtained at the G3MP2 level of theory for the title reaction through all the transition states are given in Table 3. It is clear from Table 3 that the reaction through the transition states, namely, R1-TS4, R1-TS5, R2-TS4 and R2-TS5 is found to be more exothermic compared to the other possible transition states.

Table 2. The classical barrier heights (ΔE_0 in kcal mol^{-1}) and the entropy of activation ($\Delta S^{\ddagger}$ in cal mol^{-1} K^{1}) obtained from G3MP2 level of theory

Rotamer	TS	ΔE_0	$\Delta S^{\ddagger}$
1	TS1	–2.08	15.47
	TS2	6.80	13.70
	TS3	5.52	12.88
	TS4	5.13	14.57
	TS5	2.92	15.94
	TS6	3.63	14.07
	TS7	3.60	14.23
	TS8	4.33	16.97
2	TS1	–1.56	17.00
	TS2	7.15	14.80
	TS3	3.59	10.43
	TS4	2.04	14.70
	TS5	1.75	12.45
	TS6	4.09	16.92
	TS7	3.69	14.12
	TS8	3.38	13.80

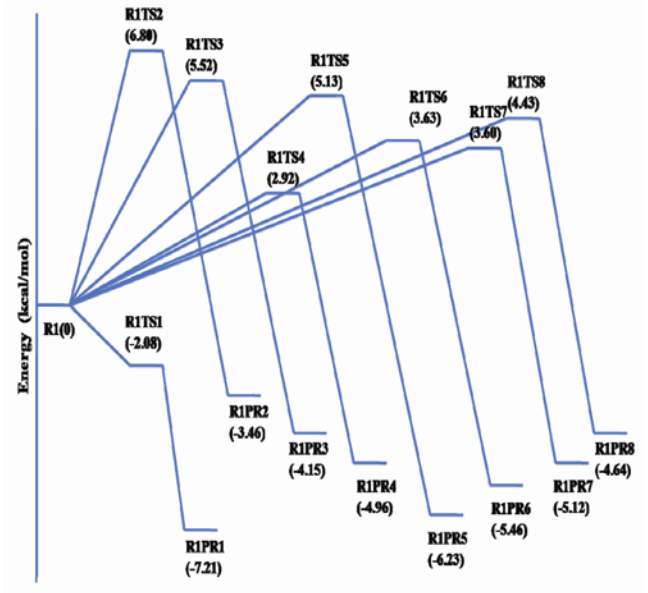

Figure 3. Energy-level diagram for the title reaction through all the transition states and all channels at G3MP2 theory for rotamer-1.

Kinetic parameters

Theoretical rate coefficients for the title reaction were calculated in the temperature range 200–400 K with 25 K intervals using CTST with Wigner tunnelling corrections coupled with the G3MP2 theory. As discussed

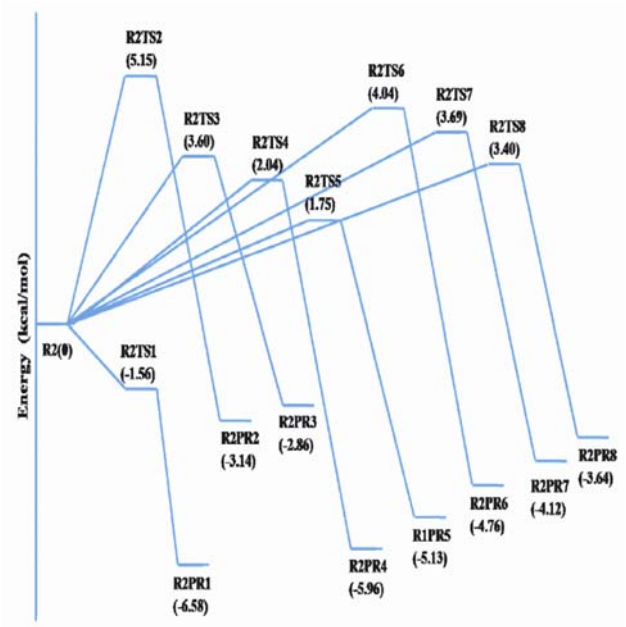

Figure 4. Energy-level diagram for the title reaction through all the transition states and all channels at G3MP2 theory for rotamer-2.

Table 3. Enthalpy (ΔH^0 (298 K) in kcal mol^{-1}), Gibbs free energy (ΔG^0 (298 K) in kcal mol^{-1}) and entropy (ΔS^0 (298 K) in cal mol^{-1} K^{-1}) of the title reaction

Rotamer	TS	ΔH^0	ΔG^0	ΔS^0
1	TS1	–24.50	–26.95	8.23
	TS2	–4.15	–5.86	5.76
	TS3	–9.02	–10.39	4.60
	TS4	–35.68	–36.63	3.18
	TS5	–35.68	–36.63	3.17
	TS6	–13.45	–15.13	5.63
	TS7	–14.55	–16.24	5.68
	TS8	–15.65	–17.36	5.74
2	TS1	–24.50	–26.95	8.24
	TS2	–4.86	–6.73	6.28
	TS3	–6.94	–8.40	4.88
	TS4	–37.15	–37.97	2.77
	TS5	–37.15	–37.98	2.77
	TS6	–15.55	–17.15	5.39
	TS7	–15.65	–17.24	5.34
	TS8	–15.60	–17.18	5.29

Table 4. Arrhenius parameters for the title reaction $CH_3CH_2CH=CHCHO$ with OH at G3MP2 theory and both models (HO and HR) used in the calculations

	G3MP2		Experiment[10]	
Model	A (cm^3 mol^{-1} s^{-1})	E_a/R (K)	A (cm^3 mol^{-1} s^{-1})	E_a/R (K)
HR	$(2.57 \pm 0.33) \times 10^{-13}$	$-(1482 \pm 53)$	$(7.9 \pm 1.2) \times 10^{-12}$	$-(510 \pm 53)$
HO	$(2.6 \pm 0.33) \times 10^{-13}$	$-(1165 \pm 41)$		

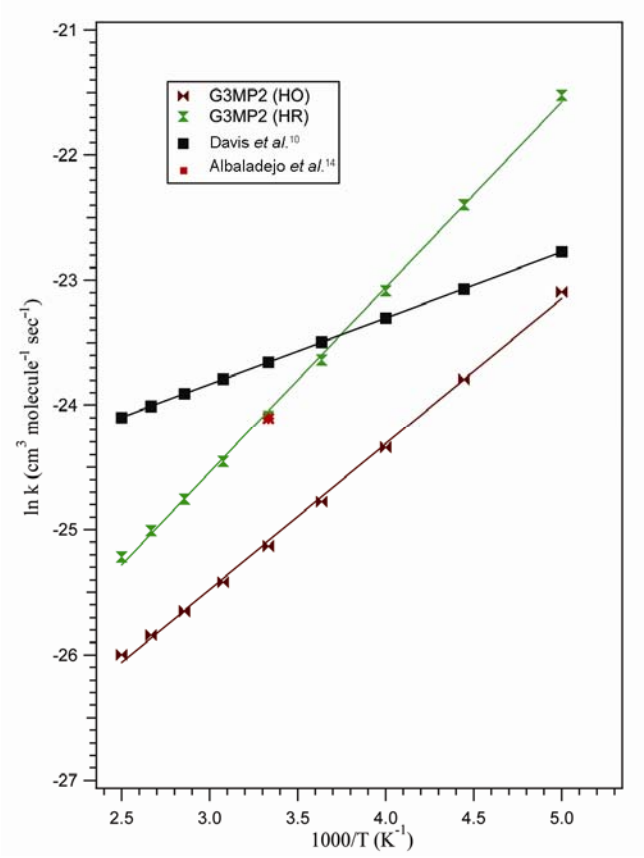

Figure 5. Arrhenius plot for the rate coefficient data obtained for the title reaction over the temperature range 200–400 K at G3MP2 theory and the available experimental data. HO, Harmonic oscillator; HR, Hindered rotor and FR, Free rotor.

earlier, the reaction goes through five main channels, namely C1, C2, C3, C4 and C5 [hydrogen abstraction from aldehyde, methyne, methyne, methylene and methyl groups results in five different product radicals: $CH_3CH_2CH=CHCO$, $CH_3CH_2CH=CCHO$, $CH_3CH_2C=CHCHO$, $CH_3CHCH=CHCO$, $CH_2CH_2CH=CHCO$ respectively]. A total of 16 transition states (eight for each rotamer) for this reaction were found. Therefore, rate coefficients for the reaction through all the transition states were computed and then they were added to get the global rate coefficient at each level of theory as follows:

$$k_{\text{global}}(T) = w_{R1}k_{R1} + w_{R2}k_{R2}, \quad (3)$$

where $k_{R1} = k_{R1C1} + k_{R1C2} + k_{R1C3} + k_{R1C4} + k_{R1C5}$, $k_{R2} = k_{R2C1} + k_{R2C2} + k_{R2C3} + k_{R2C4} + k_{R2C5}$. k_{R1} and k_{R2} are the total rate coefficients for rotamer R1 and R2 respectively. k_{R1C1}, k_{R1C2}, k_{R1C3}, k_{R1C4} and k_{R1C5} are the rate coefficients for the rotamer R1 through C1, C2, C3, C4 and C5 reaction channels respectively. Similarly, k_{R2C1}, k_{R2C2}, k_{R2C3}, k_{R2C4} and k_{R2C5} are the rate constants for the rotamer R2 through C1, C2, C3, C4 and C5 reaction channels respectively. w_{R1} and w_{R2} are the weight factors of each rotamer (estimated using Boltzmann distribution). In computing the rate coefficients, the torsional motion (for the lower normal mode frequencies wherever necessary) was treated with two models, namely harmonic oscillator (HO) and hindered rotor (HR) as described[24]. The computed rate coefficients using the G3MP2 theory and models are plotted in Figure 5. The absolute rate coefficient reported by Albaladejo *et al.*[14] is also shown in the plot. The experimentally measured rate coefficient by Davis *et al.*[10] is also plotted in Figure 5. It is clear from the figure that the trend followed by the theoretically computed rate coefficient is deviated across the temperature range when compared with the experimental data. However, the rate coefficients obtained in our study are well in the vicinity of the experimentally determined values. The Arrhenius parameters obtained by an unweighted linear least squares fit to all the data are given in Table 4 along with the available experimental data. It can be observed from Table 4 that the pre-exponential factors predicted with the G3MP2 theory are lower by almost an order of magnitude when compared to the experimentally determined ones. Also, the activation energy predicted with the G3MP2 theory is lower by about 1 k cal mol^{-1}. However, experimentally one can measure the rate coefficient but not the Arrhenius parameters and it is always worth comparing the rate coefficients. The rate coefficients for the title reaction obtained with the G3MP2 theory and models for all the transition states at 300 K are give in Table 5. Contribution of each rotamer to the global rate coefficient is also given in the table. It is clear from Table 5 that rotamer-1 contributes much (almost 73% with HR model and 72% with HO model) towards the global rate coefficient and the rest is from rotamer-2. Rate coefficient calculated at 300 K using G3MP2 theory and HR model is 3.46×10^{-11} cm^3 mol^{-1} s^{-1}, which is reasonably closer to the experimentally determined value 4.3×10^{-11} cm^3 mol^{-1} s^{-1} by Davis *et al.*[10].

Table 5. The rate coefficients for the reaction through all the transition states at 300 K with G3MP2 level of theory with Wigner tunnelling corrections and with HR and FR models

	Transition state									
Rotamer	TS1	TS2	TS3	TS4	TS5	TS6	TS7	TS8	Sum (%)	Global
HO										
1 [50.3%][a]	1.72×10^{-11}	2.92×10^{-18}	3.44×10^{-16}	5.98×10^{-15}	7.51×10^{-17}	5.45×10^{-16}	5.50×10^{-16}	2.24×10^{-15}	0.86×10^{-11} (72%)[b]	1.21×10^{-11}
2 [49.7%][a]	7.03×10^{-12}	1.46×10^{-18}	1.50×10^{-17}	1.65×10^{-15}	2.32×10^{-17}	2.10×10^{-16}	4.39×10^{-16}	4.84×10^{-16}	0.35×10^{-11} (28%)[b]	
HR										
1 [50.3%][a]	4.98×10^{-11}	1.58×10^{-19}	3.18×10^{-17}	1.24×10^{-16}	3.02×10^{-15}	2.16×10^{-16}	4.51×10^{-17}	1.99×10^{-16}	2.52×10^{-11} (73%)[b]	3.46×10^{-11}
2 [49.7%][a]	1.72×10^{-11}	5.6×10^{-20}	1.55×10^{-18}	3.54×10^{-17}	8.11×10^{-15}	7.77×10^{-18}	4.37×10^{-17}	6.28×10^{-17}	9.36×10^{-12} (27%)[b]	

[a]Values in square bracket correspond to the weight factors of the particular rotamer.
[b]Values in parenthesis correspond to the contribution of the particular rotamer towards the global rate coefficient.

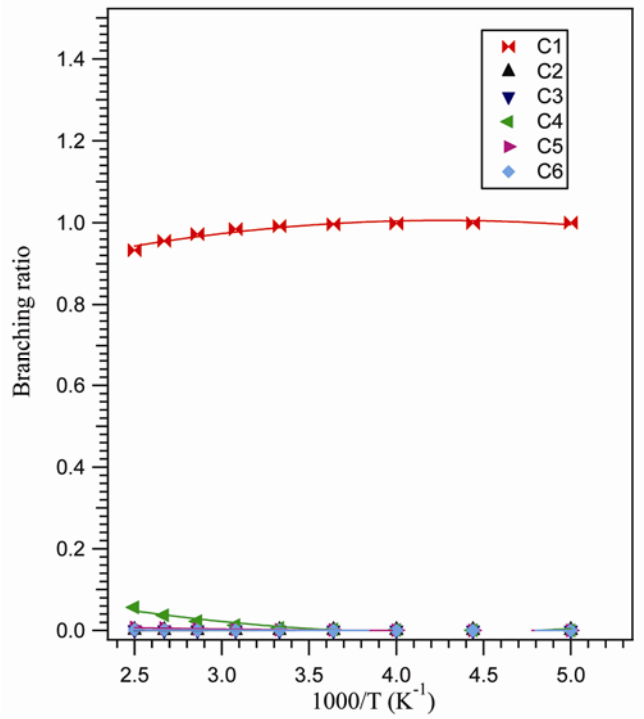

Figure 6. Branching ratios for the reaction channels C1–C6 of the reaction (E)-2-pentanal with OH radical between the temperature range 200–400 K. The kinetic parameters used in the plot were obtained at G3MP2 theory with HR model. Solid lines are the fit to the data.

Branching ratio

To get a clear picture about the contribution of each reaction channel, we have calculated the temperature-dependent branching ratios for all the possible channels, namely C1–C6 for both the rotamers (R1 and R2) within the temperature range 200–400 K (Figure 6). From the temperature-dependent branching ratios shown in Figure 6, it is clear that the aldehydic channel C1 (–CHO group) is the dominant one and contributes maximum (almost 98%) towards the global rate coefficient at a given temperature in the range 200–400 K. Available rate coefficients reported for the reaction of OH radicals with *n*-propanal, 2-propenal, *n*-butanal, and (E)-2-butenal, *n*-pentanal and (E)-2-pentenal (this work) are given in Table 6. It is cleared that the measured rate coefficients seem to be independent of the number of carbon atoms in the molecule. No systematic trend is observed either in the pre-exponential factors or in the activation energies either with the increase in the number of carbon atoms or a double bond in the molecule. One interesting feature among all these reactions is that the activation energies are negative, irrespective of the presence or absence of the double bond.

Atmospheric implications

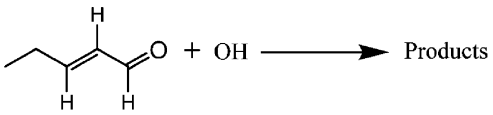

(E)-2-Pentenal

(E)-2-Pentenal degrades in the atmosphere via gas-phase reactions with OH, NO_3 and O_3 and by UV photolysis. Presence of ethyl group leads to the enhancement of the reactivity of the double bond, but presence of an adjacent carbonyl group provides a deactivating effect on the reactivity of the double bond toward OH, resulting in decrease in the reactivity of the double bond[12]. Hence the reaction mainly goes through abstraction of hydrogen. The plausible mechanism is given in Figure 1, for the OH

Table 6. Comparison of the experimentally measured rate coefficients of the reactions of OH with *n*-propanal, 2-propanal, *n*-butanal, (E)-2-butenal, *n*-pentanal and (E)-2-pentenal

Molecule	Temperature (K)	k (T)		k (298 K) ($cm^3\ mol^{-1}\ s^{-1}$)	Reference
		A ($cm^3\ mol^{-1}\ s^{-1}$)	E_a/R (K)		
n-propanal	298	a	a	$(1.71 \pm 0.23) \times 10^{-11}$	25
2-propenal	243–372	$(6.55 \pm 0.12) \times 10^{-12}$	-333 ± 54	$(6.03 \pm 0.12) \times 10^{-11}$	12
n-butanal	258–422	$(5.71 \pm 0.28) \times 10^{-12}$	-817 ± 60	$(2.06 \pm 3.0) \times 10^{-11}$	25
2-butenal	298	a	a	$(1.70 \pm 0.53) \times 10^{-11}$	11
	243–372	$(5.77 \pm 1.13) \times 10^{-12}$	-533 ± 58	$(3.55 \pm 0.30) \times 10^{-11}$	12
n-pentanal	253–410	$(6.29 \pm 0.18) \times 10^{-12}$	-896 ± 40	$(2.86 \pm 0.18) \times 10^{-11}$	25
(E)-2 pentenal	253–410	$(7.9 \pm 1.2) \times 10^{-12}$	-510 ± 40	$(4.3 \pm 0.6) \times 10^{-11}$	10
	200–400	$(2.88 \pm 0.46) \times 10^{-13}$	-1152 ± 51	1.64×10^{-11}	Present work

[a]Data not available in the literature.

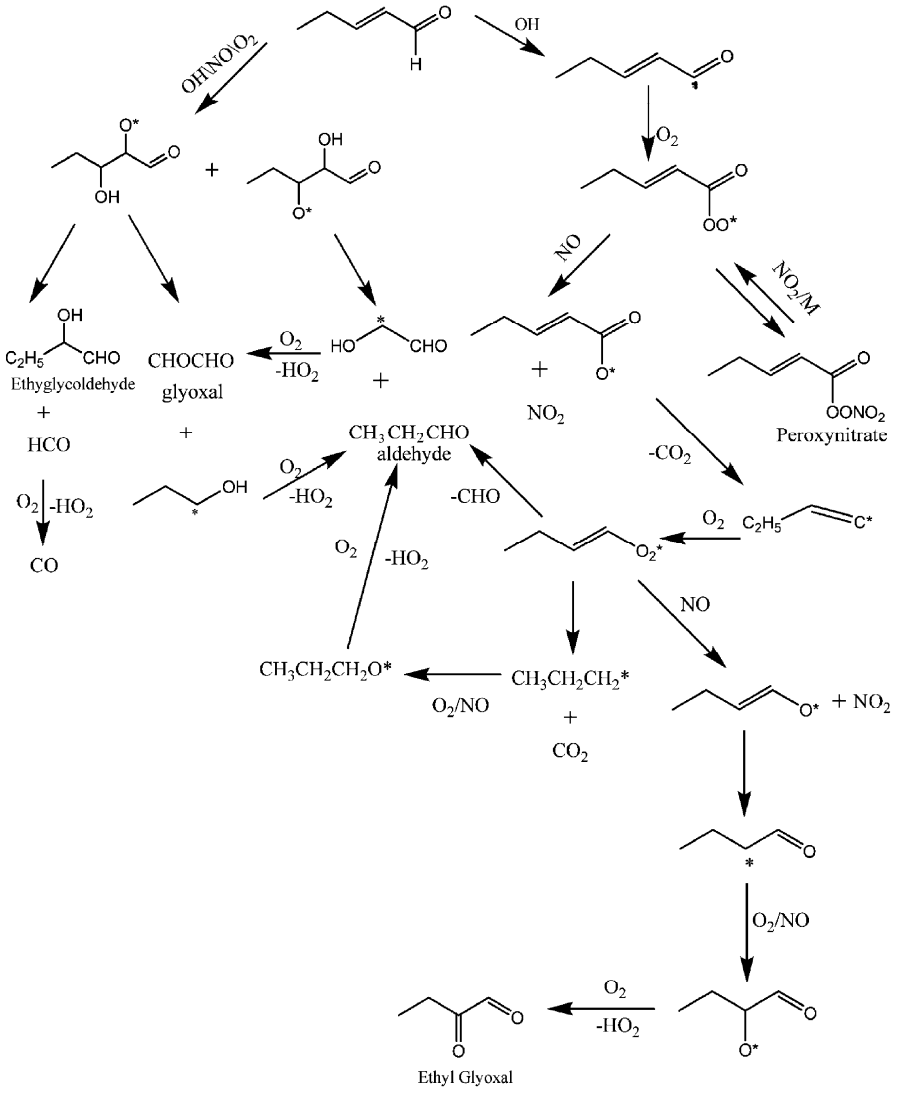

Figure 7. Mechanism for the OH initiated atmospheric oxidation of (E)-2-pentenal in the nitrogen-rich experiment. '∗' represents the radical.

initiated atmospheric oxidation of (E)-2-pentenal in the nitrogen-rich environments. Products observed in the OH-initiated oxidation of (E)-2-pentenal are propanaldehyde (CH_3CH_2CHO), glyoxal (CHOCHO), peroxynitrate ($CH_3CH_2CHCHCOONO_2$), ethyl glyoxal (CH_3CH_2-COCHO) and ethyl glycoldehyde (CH_3CH_2COCHO). The photo-oxidation mainly occurs by abstraction; still contribution from addition to the double bond is possible. None of the stable products formed is long-lived in the atmosphere and is generally lost in the troposphere. Atmospheric

lifetime of (E)-2-pentenal was calculated using the rate coefficient obtained with the G3MP2 theory with HR model to be 5 h, which is in excellent agreement with the experimentally determined value (4 ± 0.5 h) by Davis *et al.*[10].

Hence, here we have obtained the kinetic parameters for the reactions of abstraction of hydrogen from (E)-2-pentanal by the hydroxyl (OH) radical through all the possible reaction channels by coupling G3MP2 theory with the CTST. In an earlier theoretical investigation by Grosjean *et al.*[15], they have not explored all these reaction channels and the study is based only on the semi-empirical methods.

Conclusion

The kinetic parameters for the reaction of OH radical initiated atmospheric oxidation of (E)-2-pentenal were obtained with G3MP2 theory coupled with CTST with Wigner tunnelling corrections. The geometries of all the stationary points on the PES and all the possible transition states were explored and the contribution of each transition state to the global rate coefficient has been computed. The temperature-dependent rate coefficient for this reaction in the temperature range 200–400 K is deduced to be $(2.57 \pm 0.33) \times 10^{-13} \exp[(1482 \pm 53)/T]$ cm^3 mol^{-1} s^{-1}. The lifetime of the test molecule computed with the G3MP2 theory was found to be 5 h. To understand the contribution of aldehydic hydrogen to the global rate coefficient, experimental investigations using a deuterated test molecule are necessary and such experiments have been planned in our laboratory.

1. Guenther, A., Geron, C., Pierce, T., Lamb, B., Harley, P. and Fall, R., Natural emissions of non-methane volatile organic compounds, carbon monoxide, and oxides of nitrogen from North America. *Atmos. Environ.*, 2000, **34**, 2205–2230.
2. Guenther, A. *et al.*, A global model of natural volatile organic compound emissions. *J. Geophys. Res. [Atmos.]*, 1995, **100**, 8873–8892.
3. Simpson, D., Guenther, A., Hewitt, C. N. and Steinbrecher, R., Biogenic emissions in Europe 1. Estimates and uncertainties *J. Geophys. Res. [Atmos.]*, 1995, **100**, 22875–22890.
4. UNFCCC, Report of the conference of the parties, on its third session, held at Kyoto from 1 to 11 December 1997. Kyoto Protocol to the United Nations Framework Convention on Climate Change. Document FCCC/CP/1997/7/Add.1; http://www.unfccc.de
5. de Gouw, J. A., Howard, C. J., Custer, T. G. and Fall, R., Emissions of volatile organic compounds from cut grass and clover are enhanced during the drying process. *Geophys. Res. Lett.*, 1999, **26**, 811–814.
6. Hatanaka, A., The biogeneration of green odour by green leaves. *Photochemistry*, 1993, **34**, 1201–1218.
7. Schnitizler, J. P. *et al.*, Emission of biogenic volatile organic compounds: an overview of field, laboratory and modelling, studies performed during the tropospheric research program (TFS) 1997–2000. *J. Atmos. Chem.*, 2002, **42**, 159–177.
8. Nakamura, S. and Hatanaka, A., Green-leaf-derived C6-aroma compounds with potent antibacterial action that act on both Gram-negative and Gram-positive bacteria. *J. Agric. Food Chem.*, 2002, **50**, 7639–7644.
9. Astridkiendlet-Scharr, Qizhang, Thorstenhohaus, Einhardkleist, Amewu Mensah, Christianspindler, Ricardauerlings, Ralftillmann and Andjurgenwildt, Aerosol mass spectrometric features of biogenic SOA: observations from a plant chamber and in rural atmospheric environments. *Environ. Sci. Technol.*, 2009, **43**, 8166–8172.
10. Devis, M. E., Gillies, M. K., Ravishankara, A. R. and Burkholder, J. B., Rate coefficients for the reaction of OH with (E)-2-pentenal, (E)-2-hexenal, and (E)-2-heptenal. *Phys. Chem. Chem. Phys.*, 2007, **9**, 2240–2248.
11. Orlando, J. J. and Tyndall, G. S., Mechanisms for the reactions of OH with two unsaturated aldehydes: crotonaldehyde and acrolein. *J. Phys. Chem. A.*, 2002, **106**, 12252–12259.
12. Magneron, I., The´venet, R., Mellouki, A., Le Bras, G., Moortgat, G. K. and Wirtz, K., A study of the photolysis and OH-initiated oxidation of acrolein and *trans*-crotonaldehyde. *J. Phys. Chem. A.*, 2002, **106**, 2526–2537.
13. Cabanas, B., Salgado, S., Martin, P., Baeza, M. T. and Martinez, E., Night-time atmospheric loss process for unsaturated aldehydes: reaction with NO_3 radicals. *J. Phys. Chem. A*, 2001, **105**, 4440–4445.
14. Albaladejo, J., Ballesteros, B., Jimenez, E., Martin, P. and Martinez, E., A PLP–LIF kinetic study of the atmospheric reactivity of a series of C_4–C_7 saturated and unsaturated aliphatic aldehydes with OH. *Atmos. Environ.*, 2002, **36**, 3231–3239.
15. Grosjean, D. and Williams, E. L., Environmental persistence of organic compounds estimated from structure-reactivity and linear free-energy relationships. Unsaturated aliphatics. *Atmos. Environ. Part A. General Topics*, 1992, **26**(8), 1395–1405.
16. Frisch, R. C. *et al.*, Gaussian 03, Revision C.02, Gaussian, Inc., Wallingford CT, 2004.
17. Møller, C. and Plesset, M. S., Note on an approximation treatment for many-electron systems. *Phys. Rev.*, 1934, **46**, 618–622.
18. Denninggton II, R., Keith, T., Millam, J., Eppinnett, K., Hovell, W. L. and Gilliand, R., GaussView, Version 3.09, Seemichem Inc., Shawnee Mission, KS, 2003.
19. Curtiss, L. A., Redfern, P. C., Raghavachari, K., Rassolov, V. and Pople, J. A., Gaussian-3 theory using reduced Møller-Plesset order. *J. Chem. Phys.*, 1999, **100**, 4703.
20. Wright, M. R., *Fundamental Chemical Kinetics: An Exploratory Introduction to the Concepts*, Ellis Horwood, Chichester, 1999.
21. Mora-Diez, N. and Boyd, R. J., A computational study of the kinetics of the NO_3 hydrogen-abstraction reaction from a series of aldehydes (XCHO: X = F, Cl, H, CH_3). *J. Phys. Chem. A*, 2002, **106**, 384.
22. Ogura, T., Miyoshi, A. and Koshi, M., Rate coefficients of H-atom abstraction from ethers and isomerization of alkoxyalkyl peroxy radicals. *Phys. Chem. Chem. Phys.*, 2007, **9**, 5133.
23. Wigner, E. P., *Z. Phys. Chem.* (*Leipzig*), 1932, **Bl9**, 203.
24. Chuang, Y.-Y. and Truhlar, D. G., Statistical thermodynamics of bond torsional modes. *J. Chem. Phys.*, 2000, **112**, 1221.
25. Semmes, D. H., Ravishankara, A. R., Gump-Perkins, C. A. and Wine, P. H., Kinetics of the reactions of hydroxyl radical with aliphatic aldehydes. *Int. J. Chem. Kinet.*, 1985, **17**, 303.

ACKNOWLEDGEMENTS. All calculations reported in this article were carried out at the High Performance Computing Environment, Indian Institute of Technology Madras. We thank the staff of HPCE, especially, Mr Ravichandaran for valuable support. B.U. thanks Dr Mohammad Akbar Ali for useful discussions.